Applied Surface Science 531 (2020) 147311

Contents lists available at ScienceDirect

Applied Surface Science

journal homepage: www.elsevier.com/locate/apsusc

Effective usage of 2D MXene nanosheets as solid lubricant – Influence of contact pressure and relative humidity

Max Marian[a,*], Gui Cheng Song[b], Bo Wang[b], Victor M. Fuenzalida[c], Sebastian Krauß[d], Benoit Merle[d], Stephan Tremmel[a], Sandro Wartzack[a], Jinhong Yu[b], Andreas Rosenkranz[e,*]

[a] Engineering Design, Friedrich-Alexander-Universität Erlangen-Nürnberg (FAU), Erlangen, Germany
[b] Key Laboratory of Marine New Materials and Related Technology, Zhejiang Key Laboratory of Marine Materials and Protection Technology, Ningbo Institute of Material Technology & Engineering, Chinese Academy of Sciences, Ningbo 315201, People's Republic of China
[c] Department of Physics, FCFM, Universidad de Chile, Santiago, Chile
[d] Materials Science & Engineering I, Interdisciplinary Center for Nanostructured Films, Friedrich-Alexander-Universität Erlangen-Nürnberg (FAU), Erlangen, Germany
[e] Department of Chemical Engineering, Biotechnology and Materials, FCFM, Universidad de Chile, Santiago, Chile

ARTICLE INFO

Keywords:
MXene-nanosheets
Contact pressure
Relative humidity
Friction reduction
Wear reduction

ABSTRACT

Newly emerging $Ti_3C_2T_x$–nanosheets (MXenes) have attracted considerable attention in energy storage, catalysis and, more recently, tribology. MXene nanosheets are characterized by a weakly-bonded multi-layered structure with self-lubricating ability, making them a suitable candidate for solid lubrication. This contribution aims at addressing for the first time their application in higher loaded steel/steel dry sliding contacts by investigating the influence of contact pressure and relative humidity on friction and wear performance. Compared to the uncoated reference, a 2.3-fold friction reduction and a 2.7-fold reduction of the wear volume were verified for MXene-coated specimens for moderate contact pressures and low relative humidity. This was due to the in-situ formation of a compacted tribo-film consisting of densified $Ti_3C_2T_x$–nanosheets. In contrast, too high pressures induced a partial rupture of the wear-protecting tribo-layer, thus reducing its beneficial effects. Additionally, no beneficial effects regarding friction and/or wear were found at higher relative humidities, which was correlated with the expansion of the basal spacings. Therefore, this study summarizes favorable operating conditions for MXene nanosheets when used as solid lubricant to improve friction and/or wear thus making them excellent candidates for advanced, next-generation solid lubricants.

1. Introduction

The discovery of graphene with its remarkable physical properties can be considered as the initiation of the field of 2–dimensional materials [1–3]. Since then, different 2D materials including hexagonal boron nitrides, transition metal dichalcogenides and metal oxides have experienced great attention in research community [4–7]. Since 2011, the family of 2-dimensional materials has been significantly expanded by the early transition metal carbides and/or carbonitrides based upon MAX-phases and named s MXenes as introduced by NAGUIB et al. [8]. The main process route to produce MXenes is to remove the A layers of $M_{n+1}AX_n$ (M: early transition metal, A: group IIIA or IVA element and X: C or N with n = 1, 2 or 3) by etching [8,9]. MXenes in general and Ti_3C_2 in particular, which can be considered as the most studied MXene so far, have gained considerable attention due to their resulting physical properties, thus leading to an outstanding material's performance in different fields such as energy storage, supercapacitors and catalysis [9–13].

Apart from that, MXenes are particularly interesting for tribological applications due to their graphite-like structure, low shear strength and self-lubrication ability [14]. This aspect has also been confirmed by theoretical studies using density functional calculations and molecular dynamic simulations by ZHANG et al. [15]. However, the usage of MXenes in the context of tribology is surprisingly underexplored, although bearing tremendous potential as a lubricant additive, a reinforcement phase in composite materials and a solid lubricant [16].

ZHANG et al. [17] demonstrated beneficial effects of the usage of Ti_3C_2-nanosheets when mixing them with ultra-high molecular weight polyethylene to create a Ti_3C_2/polymer-composite. Besides a slightly increased hardness, improved yield strength and creep resistance, the Ti_3C_2/polymer-composites showed a reduced coefficient of friction (*COF*) and superior wear performance. Recently, MAI et al. [18]

* Corresponding authors.
E-mail addresses: marian@mfk.fau.de (M. Marian), arosenkranz@ing.uchile.cl (A. Rosenkranz).

https://doi.org/10.1016/j.apsusc.2020.147311
Received 29 March 2020; Received in revised form 25 May 2020; Accepted 18 July 2020
Available online 25 July 2020

investigated the tribological behavior of Ti_3C_2/copper-composite coatings fabricated by electrodeposition. The composites revealed a significant friction reduction of up to 46% as well as a tremendous reduction of the wear rate by a factor of 19. By microscopy and Raman spectroscopy, this was attributed to the formation of a compact, self-lubricating film, which reduced the probability of having a metal–metal contact and is easy to shear.

YANG et al. [19] mixed Ti_3C_2-nanosheets with paraffin oil and studied their ability to act as a lubricant additives dependent on the weight percentage and the normal load. The greatest friction reduction was found for a concentration of 1 wt-%, which was explained by the possibility to form a self-laminating film under compressive stresses. Furthermore, they demonstrated that the wear behavior can be greatly improved [19]. Similar conclusions with respect to the concentration were presented by ZHANG et al. [20]. The usage of 1 wt–% $Ti_3C_2(OH)_2$-nanosheets in a base oil resulted in the greatest friction and wear reduction. Additionally, a certain critical normal load needed to be exceeded to generate a low and stable *COF* over time. However, exceeding these critical loads led to adverse effects [21]. LIU et al. [22] studied the tribological behavior of a Poly-(alpha)-olefin oil mixed with $Ti_3C_2T_x$-nanosheets as a function of the concentration and the degree of exfoliation. In agreement with the aforementioned reports, the maximum friction and wear reduction was found for a concentration of 0.8 wt-%. Furthermore, the authors revealed the important influence of the degree of exfoliation with the best results obtained for highly exfoliated nanoparticles.

LIAN et al. [14] applied a 200 nm film of Ti_3C_2-flakes on copper disks by spray coating with the overall idea to use it as a solid lubricant. Ball-on-disk experiments demonstrated the potential to reduce friction (up to a factor of 3.5) and wear (one order to magnitude) significantly. ROSENKRANZ et al. [23] deposited a thin layer of $Ti_3C_2T_x$-nanosheets on stainless steel by drop casting and studied the frictional behavior under dry friction against an alumina ball. A pronounced three fold reduction in the *COF* combined with a significant reduction of adhesional, abrasive and tribochemical wear was observed. GUO et al. [24] studied frictional and adhesional properties of MXene–nanosheets using atomic force microscopy as a function of the applied normal force, temperature and pressure. Mxene-nanosheets revealed better frictional and adhesional properties at higher temperatures, which were also proportional to the applied pressure. YIN et al. [25] have investigated MXene and MXene/nanodiamond coatings under dry conditions and low contact pressures (10 and 20 MPa) when rubbing against mainly polymeric counter-bodies. For the purely MXene coating, they observed stable *COF*s around 0.3 for PTFE and almost no detectable wear, which was traced back to the formation of a tribofilm consisting of densified MXene–nanoflakes. In case of the MXene/nanodiamond coating, *COF*s of about 0.16 have been observed with an ultra-smooth wear track. A detailed investigation via focussed ion beam and transmission electron microscopy revealed the formation of a nano-structured tribofilm. MARIAN et al. [26] applied $Ti_3C_2T_x$ nanosheets (Mxenes) as a solid lubricant to dry-running thrust ball bearings under ambient conditions. They verified a reduction of frictional torque by a factor of 3.2, an extension of service life by about 2.1 times and a decrease of linear cumulative wear by up to 2.9 compared to uncoated references.

Most previous studies on MXene–nanosheets in tribological applications have been limited to very specific niche material pairings, rather low or moderate contact loads and pressures as well as constant environmental conditions. It is well known that other materials commonly used as solid lubricants such as graphite [27–30], graphene [31–33], hydrogenated diamond-like carbon [34–37], molybdenum disulphide [38–41] or boron-based materials [42–44] show not only dependencies of friction and wear behavior on working conditions (for instance contact pressure [45]), but also on environmental factors (for example humidity [46,47]).

Therefore, this contribution aims at investigating the influence of contact pressure and relative humidity, which is defined as the ratio of the partial pressure of water vapor to the equilibrium vapor pressure of water at given temperature, on the applicability of $Ti_3C_2T_x$-nanosheets as solid lubricants in steel/steel contacts as a widely used material pairing in machine elements and engine components.

2. Materials and methods

2.1. Materials

The initial Ti_3AlC_2-powder was purchased from FORSMAN SCIENTIFIC Co. Ltd., Beijing (China). For synthetization of the multi-layer $Ti_3C_2T_x$-nanosheets, Ti_3AlC_2-powder (10 g) was immersed in 100 mL of a 40% hydrofluoric acid solution. The mixture was stirred for three minutes and then kept at room temperature for two hours. The as-prepared suspension was then washed using deionized water several times until reaching a pH above 6 and subsequently centrifuged to separate the powder. Afterwards, the washed powder was filtered under vacuum conditions and dried at room temperature for 24 h.

For deposition on the steel substrates, the $Ti_3C_2T_x$-nanosheets were dispersed in acetone with a concentration of 1.2 mg/ml. Good dispersion was ensured by ultrasonication (BANDELIN, Sonorex TK 52H, 60 W, 35 kHz, room temperature). Prior to drop casting, the substrates were heated to 80 °C (BINDER, FED 53) to ensure fast and complete solvent's evaporation. Subsequently, 1 000 µl were deposited onto the surface using a syringe (HAMILTON, 1000 series gastight 81420).

Commercially available 100Cr6 (1.3505, AISI 52100) bearing steel shims according to ISO 683–17 [48], hardened and tempered to 62 ± 2 HRC, with a diameter of 31 mm and a height of 5 mm were used as substrate material. The surfaces were mirror-polished in a four step-process (ATM, Saphir 500), adjusting the final DIN EN ISO 4288 [49] roughness parameters (MITUTOYO, Surftest SJ–210) as given in Table 1. Prior to MXene deposition and testing, the specimens were ultrasonically cleaned (BANDELIN, Sonorex Super RK 255H, 160 W, 35 kHz, room temperature) in acetone and isopropyl alcohol for 10 min each and blow-dried using nitrogen.

2.2. Characterization of as-fabricated $Ti_3C_2T_x$–nanosheets

The quality of the as-fabricated $Ti_3C_2T_x$–nanosheets was assessed by high-resolution transmission electron microscopy (HR-TEM; FEI, Tecnai F20) using an acceleration voltage of 200 kV. The chemical composition was measured by energy dispersive X-ray spectroscopy (TEM-EDX) using EDAX detector attached to the HR-TEM. The surface chemistry, the surface terminations and intercalated water of the as-fabricated $Ti_3C_2T_x$–nanosheets were studied by Raman spectroscopy, X-Ray photoelectron spectroscopy (XPS) and temperature programmed desorption coupled with mass spectroscopy (TPD-MS). For Raman spectroscopy (WITEC, Alpha 300 RA), an excitation wavelength of 633 nm, a grating of 300 g/mm and 10% of the maximum laser intensity were used. The spectra were collected using four seconds of integration time and a total number of 256 accumulations. The $Ti_3C_2T_x$-nanosheets were examined by XPS (PHYSICAL ELECTRONICS, model 1257) with non-monochromatic MgKα radiation, operating the source at 15 kV and 400 W. All scans were acquired using a pass energy of 44.75 eV. A wide scan with binding energies (BE) from 1000 to 0 eV using a step size of 1 eV was used for element identification (C, F, N, O, Ti and trace levels of Si, S and Al). Narrow scans of the C_{1s}, F_{1s}, O_{1s} and Ti_{2p} regions were collected under the same conditions using a step size of 0.025 eV. Data processing was performed using the MULTIPAK package. Energy correction was performed by assigning 274.8 eV to the maximum of the C_{1s} peak. The Shirley method was used for background subtraction for the C_{1s}, F_{1s}, O_{1s} regions, but this provided no good background for the Ti_{2p} region, where linear subtraction was used instead. The peaks were fitted with Lorentz–Gaussian functions, maintaining the number of curves as low as possible to provide an acceptable match: two singlets for the F_{1s} and O_{1s} regions, three singlets for the C_{1s} region, and three

Table 1
Evaluation of surface roughness parameters according to DIN EN ISO 4288 (n = 4).

R_a in µm	R_q in µm	R_z in µm	R_p in µm	R_v in µm	R_{sk} in µm	R_k in µm	R_{pk} in µm	R_{vk} in µm
0.0273 ± 0.0012	0.0353 ± 0.0007	0.2225 ± 0.0130	0.1088 ± 0.0088	0.1131 ± 0.0107	−0.0657 ± 0.1230	0.0897 ± 0,0033	0.0374 ± 0.0035	0.0408 ± 0.0032

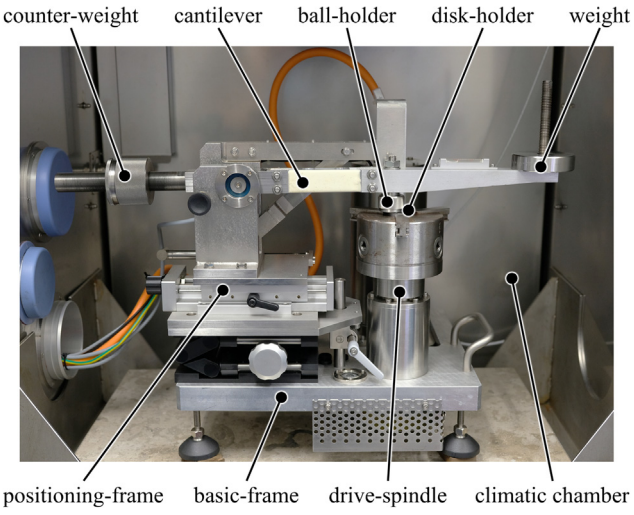

Fig. 1. Experimental set-up of the ball-on-disk-tribometer embedded in a climatic chamber.

doublets for the Ti_{2p} region. After curve fitting the figures were constructed with 0.1 eV steps. TPD–MS was performed using the 3Flex from Micromeritics equipment combined with a mass spectrometer (MKS SPECTRA PRODUCT, Cirrus 2). The sample (15–30 mg) was gradually heated in a quartz reactor at a rate of 10 °C/min until 800 °C flowing helium (100 mL/min). The water formed during the thermal treatment was identified by mass spectrometry (m/z 18). Furthermore, focused ion beam microscopy (FIB; THERMO FISHER, Scientific Helios NanoLab 600i) has been utilized to analyse the as-deposited coatings consisting of $Ti_3C_2T_x$–nanosheets. In this regard, an acceleration voltage of 5 kV, a working distance of about 4 mm and a tilting angle of 52° were used.

2.3. Tribological testing and surface characterization

A ball-on-disk tribometer (KTmfk, K-SST) as illustrated in Fig. 1 was used for tribological testing. Thereby, the disk was held by a driven three-jaw chuck. The load was applied by a weight attached to the carrier of the counter-body. The friction force was determined by the deflection of the cantilever, which was detected by strain gauges. The whole tribometer including the vibration damping frame was placed in a climatic chamber (FEUTRON, type 3436/15).

Testing was carried out in rotational sliding mode and under dry conditions. The wear radius R, sliding speed v, normal load F and maximum sliding distance SD were set to 10 mm, 0.08 m/s, 5 N and 1000 m, respectively. As counter-bodies, 100Cr6 (1.3505, AISI 52100) steel balls (grade G10, ISO 3290 [50], $R_a \leq 0.02$ µm) with diameters of 3.969 mm and 10 mm were used to reflect cases with moderate and elevated contact stresses. Thus, corresponding initial HERTZian pressures p_{Hertz} at the contact center were about 1.47 GPa and 0.80 GPa, respectively. The temperature T in the chamber was kept constant at 25 ± 2 °C, while two levels of relative humidity rh, 20 ± 5% and 80 ± 5%, were tested. These conditions have been selected to study the tribological behavior under rather extreme conditions, but still ensuring the proper function of the tribometer's climatic chamber. Three samples per pressure and humidity level were tested. For evaluation of the frictional behavior, the COF was recorded resolved over time with a data acquisition rate of 10 Hz.

To evaluate the wear behavior, the volumetric wear of the disks and balls was determined in accordance to DIN EN 1071-13 [51]. For the disks, the wear volume was assessed as the product of average cross-sectional area and the diameter of the wear track. For this purpose, the topography was measured at four positions with 90 degree offset by laser scanning microscopy (LSM; KEYENCE, VK–X200). Thereby, the average wear cross section was derived from 50 adjacent scan lines per

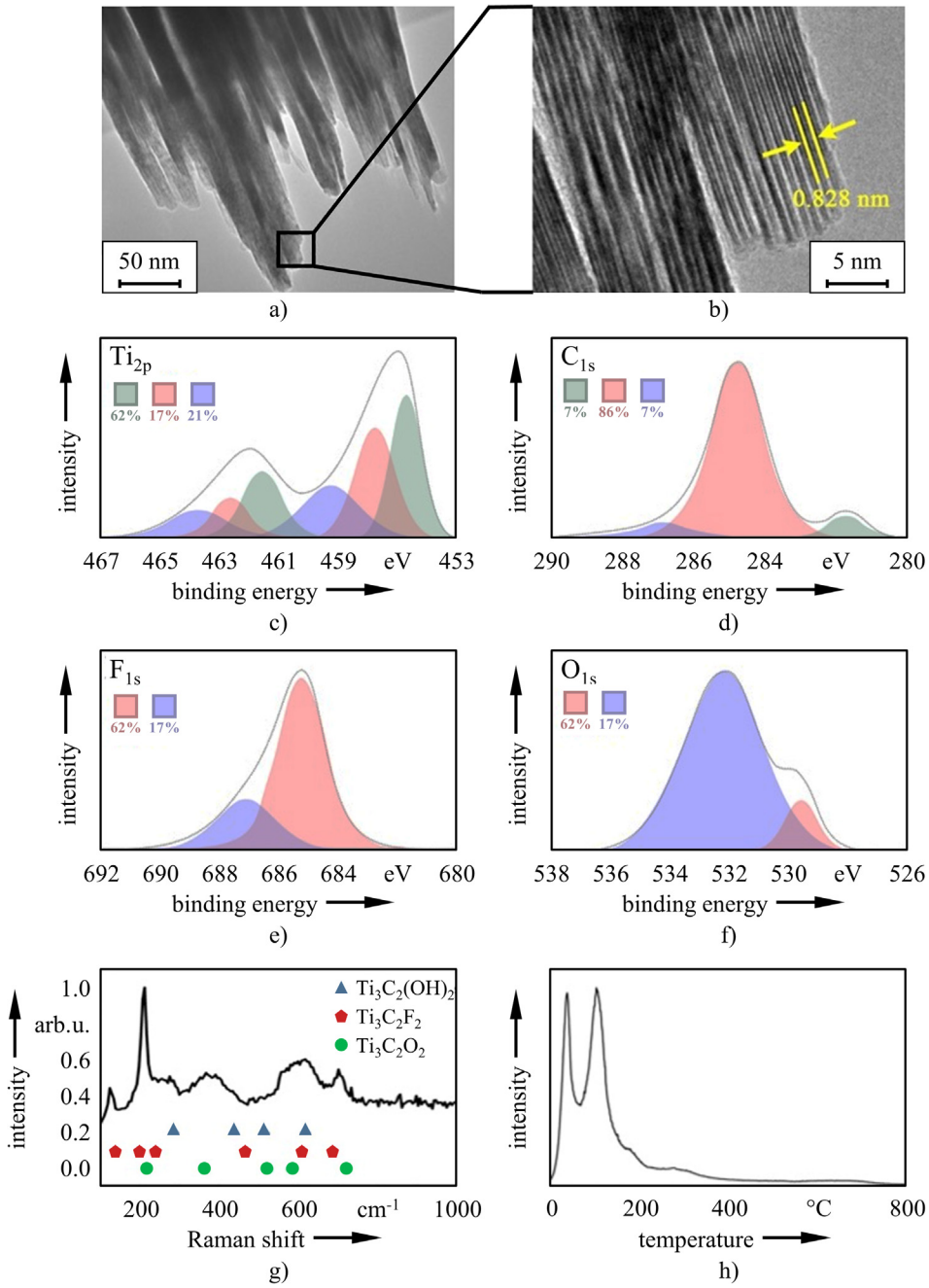

Fig. 2. Characterization of the as-synthesized $Ti_3C_2T_x$–nanosheets by TEM (a) and HR–TEM (b), XPS fitting of the narrow scans of Ti_{2p} (c), C_{1s} (d), F_{1s} (e) and O_{1s} (f), Raman spectroscopy (g) and TPD-MS (h).

measuring position and a mean value was calculated from all four positions. The wear volume of the balls was determined based upon the diameter of the wear area measured by digital light microscopy (LEICA, DM4000).

Scanning electron microscopy (SEM; ZEISS, CrossBeam 1540 EsB) of selected samples was conducted to investigate the underlying friction and wear mechanisms as well as the formation of tribo-layers. Therefore, voltages of 5 kV were applied using a working distance of about 6 mm and 8 mm. Moreover, the chemical composition of the as-deposited as well as the as-worn $Ti_3C_2T_x$-coatings and the formed tribo-layer was analyzed by Raman spectroscopy (HORIBA, LabRAM HR 800). Thereby, an excitation wavelength of 633 nm and 50% of the maximum laser intensity were used.

3. Results and discussion

3.1. Characterization

TEM and HR-TEM micrographs as depicted in Fig. 2a and b revealed the multi-layered, regular and homogenous structure of the $Ti_3C_2T_x$–nanosheets with a layer distance of 0.826 ± 0.065 nm. The used multi-layer Mxene nanosheets have in average about 80 layers and x-y-dimensions of about 1.5 µm. TEM-EDX confirmed titanium, carbon, oxygen and fluorine as main elements and reveals a minor contribution originating from aluminium, which goes hand in hand with the synthesis. The aluminium content with 0.3 wt-% was considered as to be negligible. This agreed well with previously published work [23].

The fitting of the Ti_{2p} peak fitting is revealed in Fig. 2c. The first contribution at 454.9 can be assigned to titanium carbides [52–54]. The

second contribution at 456.1 can be correlated in a general way to Ti + 2 in a variety of moieties, consisting of titanium bound to carbon and/or to oxygen or hydroxides [55]. HU et al. [56] assigned this contribution to C–Ti–OH, which matched with our results of Raman spectroscopy. This seemed reasonable since the chemical Ti state would be between the carbide and the oxide state, thus inducing intermediate binding energies. The last contribution at 457.8 and 462.7 eV was assigned by HALIM et al. [55] and HU et al. [52] to Ti + 3 and C-Ti-O. The fitting of the C_{1s} peak (Fig. 2d) demonstrated a dominant contribution (86%) centred at 284.7 eV, which was assigned to carbon in C–C chemical environment and adventitious carbon. The 281.6 eV peak is characteristic of metal carbides and associated with C–Ti–T_x [55,57], while the contribution at 286.7 eV correlates with organic components, particularly hydro-carbons [27,29]. The F_{1s} peak (Fig. 2e) showed a pronounced contribution (75%) at 685.2 eV, which was assigned to fluorinated TiO_2 (TiO_2–F_x) [58]. The second F_{1s} contribution (25%) at 687.1 eV was connected with the presence of graphite fluorides. The O_{1s} peak (Fig. 2f) showed a significant contribution (90%) at 532.2 eV, which matched well with hydroxides and therefore –OH surface terminations (C–Ti–$(OH)_x$). A minor contribution (10%) at 529.6 eV is characteristic for metal oxides and close to the values assigned to TiO_2 [59].

Raman spectroscopies (Fig. 2g) indicated pronounced peaks at 125, 212 and 701 cm^{-1} as well as broad peaks around 285, 376 and 600 cm^{-1} for the MXene nanosheets. These Raman bands fitted well with vibrations coming from $Ti_3C_2O_2$, $Ti_3C_2F_2$ and $Ti_3C_2(OH)_2$ [52,56,60]. The formation of these species was induced by the synthesis and they may slightly change the lattice spacing and the electronic structure, which resulted in additional Raman bands coming up compared to the theoretical peaks of pure Ti_3C_2 [52,56].

The water signal of the $Ti_3C_2T_x$-nanosheets as obtained by TPD-MS is depicted Fig. 2h. The first peak at 83 °C was assigned to the presence of superficial water. The second peak at 153 °C, as well as the less pronounced tail between 200 and 400 °C were traced back to absorbed/strongly bonded intercalated water [52,61,62].

The as-deposited coatings of $Ti_3C_2T_x$-nanosheets have been studied by FIB to investigate the respective interface between the steel substrate and the MXene coating (Fig. 3). Based upon this analysis, a coating's thickness of roughly 3 µm was estimated. Apart from that, it can be seen that the coating itself consists of multiple nanosheet agglomerations. For some sheets, the well-known accordion-like structure of the MXene nanosheets can be observed. Moreover, it becomes evident that more research effort needs to be dedicated towards the deposition of more homogeneous and uniform MXene coatings with improved interfacial and adhesional properties. In this regard, it would be recommendable to work on other deposition techniques such as spay techniques or electrophoretic deposition.

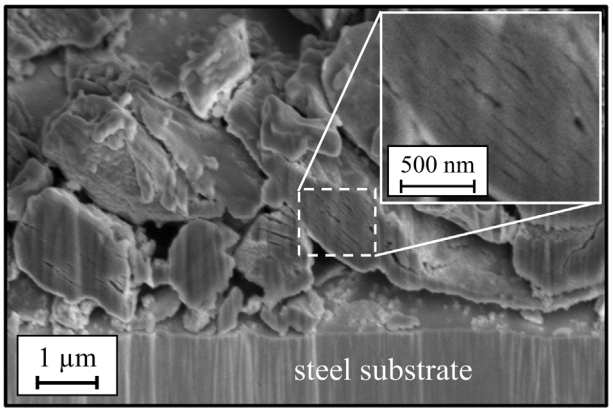

Fig. 3. FIB-cross-section of the as-deposited coating consisting of $Ti_3C_2T_x$ nanosheets.

3.2. Frictional performance

Representative *COF* curves over time (sliding cycles) for the reference and the $Ti_3C_2T_x$-coated samples at different contact pressures and relative humidities are depicted in Fig. 4, whereas the averaged values are illustrated in Fig. 5.

In case of the reference sample, the *COF* reached stable and high levels after a short running-in. For a relative humidity of 20%, these values were about 0.63 for a HERTZian pressure of 1.47 GPa (Fig. 4a and Fig. 5a, black) and about 0.36 for 0.80 GPa (Fig. 4b and Fig. 5b, black), which are typical *COF* for a steel/steel-pairing under dry sliding and respective contact pressures [63,64]. For a relative humidity of 80%, the *COF* stabilized at slightly lower values, 0.36 (Fig. 4c and Fig. 5c, black) and 0.31 (Fig. 4d and Fig. 5d, black), respectively. This is also typical for steel/steel-pairings [63,65–67] and could be traced back to the involved humidity, which facilitated the oxide layer formation on the worn steel surface and thus reduced adhesion [68,69].

In contrast, the MXene-coated samples initially featured a lower level of friction in the range of 0.21 to 0.26 (Fig. 4 and Fig. 5, blue), which was comparatively little dependent on pressure and humidity. This confirmed the self-lubricating abilities of $Ti_3C_2T_x$–nanosheets irrespective of the respective operating and/or environmental conditions. After a certain number of sliding cycles, however, the *COF* abruptly rose back to about the reference level (Fig. 5, green). Generally, this can be potentially attributed to a layer breakthrough or a reduction of the self-lubricating properties induced by mechanical stresses. As summarized in Fig. 6, the amount of sliding cycles until a significant friction increase was strongly dependent on testing conditions. The lower friction level was maintained for longer times at lower pressures and, in particular, at lower relative humidities.

3.3. Wear behavior

Characteristic line profiles of the wear track on the disks after testing are shown in Fig. 7 and calculated mean wear volumes for disks and balls are summarized in Fig. 8.

Similar to friction, wear of the steel/steel-reference also tended to be slightly lower with lower pressure and increasing relative humidity, which is typical for a steel/steel-pairing [63,64]. This could also be accounted to water promoting the oxide layer formation as well as reduced adhesion, which was consistent to previous results published in literature [63,68–70].

Despite the only temporary *COF* reduction and comparatively long overall measuring time, clear differences between reference and $Ti_3C_2T_x$-coated specimens were distinguished regarding their wear behavior. Furthermore, a strong dependency on operating and environmental conditions was observed. For lower relative humidity, a significantly less pronounced wear track could be observed on the disks (Fig. 7a and b). While a reduction by a factor of roughly 2 was observed on the disks (Fig. 8a), the wear volume on the balls hardly differed from the reference at the higher pressure (Fig. 8e). For the lower pressure, the wear volume on the disks was decreased by a factor of 1.8 (Fig. 8b) and by a factor of 3.4 on the balls (Fig. 8f). The Raman spectrum recorded in the wear track revealed four peaks of $Ti_3C_2T_x$ ranging between 120 and 600 cm^{-1}, which were also observed in the Raman spectrum of the pristine, unworn MXene-coating (Fig. 9). Consequently, the induced decrease of friction and wear can be attributed to the formation of a tribo-film consisting of densified MXene nanosheets, which is believed to be easy to be sheared and reduced the probability of metal-to-metal contact. As can be seen in corresponding SEM-micrographs, the tribo-film was ruptured in the case of higher pressure (Fig. 10), but was almost formed over the entire contact area in the case of lower pressure (Fig. 11).

While there was hardly any significant difference between reference and $Ti_3C_2T_x$-coated specimens at higher relative humidity and high pressure (Fig. 7c, Fig. 8c and g), the opposite was true at higher

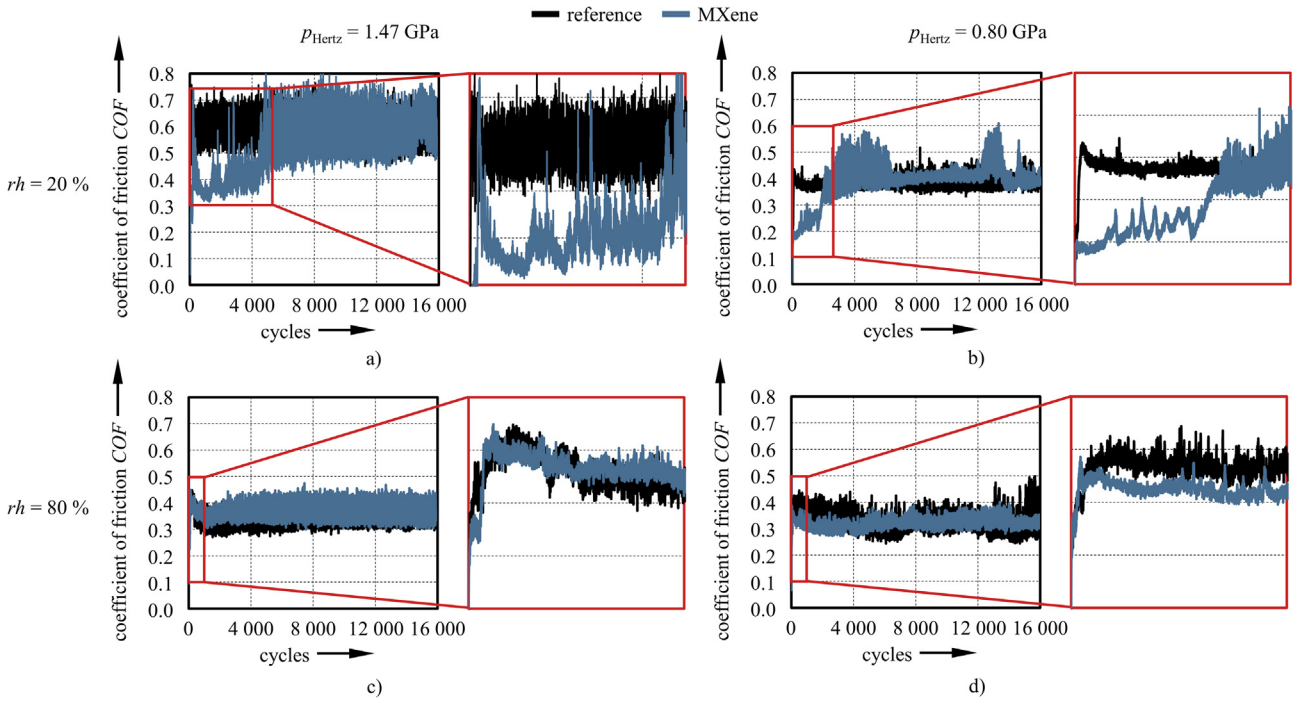

Fig. 4. Representative *COF* curves versus sliding cycles for reference (black) and $Ti_3C_2T_x$-coated (blue) specimens with an HERTZian pressure of p_{Hertz} = 1.47 GPa and at a relative humidity of *rh* = 20% (a), p_{Hertz} = 0.80 GPa and *rh* = 20% (b), p_{Hertz} = 1.47 GPa mm and *rh* = 80% (c), p_{Hertz} = 0.80 GPa and *rh* = 80% (d). Additionally, magnified views of the initial sliding cycles with pronounced friction reduction are shown.

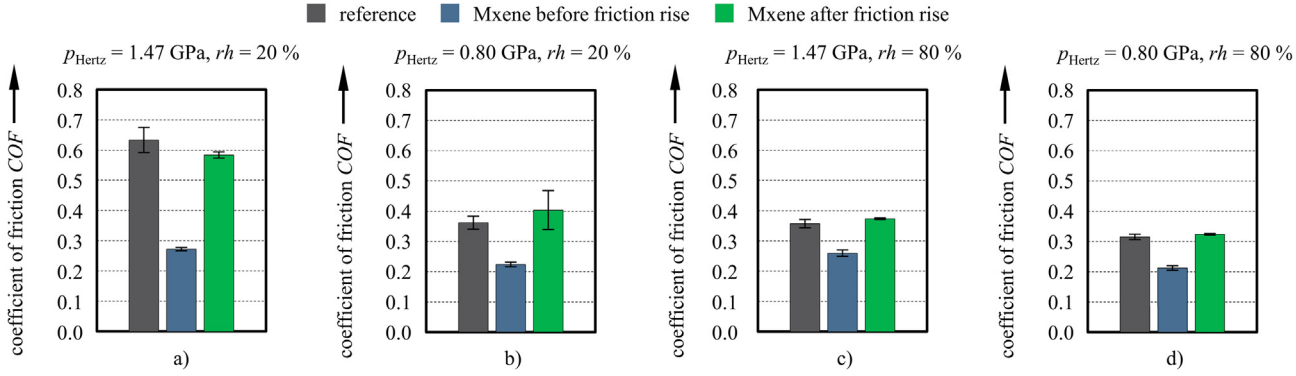

Fig. 5. Averaged *COF* (*n* = 3) for reference (grey) and $Ti_3C_2T_x$-coated specimens prior to (dark blue) and after (green) the frictional rise with an HERTZian pressure of p_{Hertz} = 1.47 GPa and at a relative humidity of *rh* = 20% (a), p_{Hertz} = 0.80 GPa and *rh* = 20% (b), p_{Hertz} = 1.47 GPa mm and *rh* = 80% (c), p_{Hertz} = 0.80 GPa and *rh* = 80% (d).

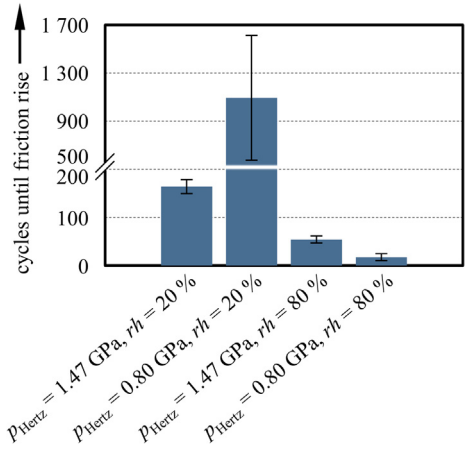

Fig. 6. Cycles until friction increase (*n* = 3) of the $Ti_3C_2T_x$-coated specimens dependent on the contact pressure and the relative humidity.

humidity and lower pressure. For these conditions, the MXene–coating even had adverse effects with very pronounced wear marks (Fig. 7d), especially in the contact centre, and a wear volume on the disks that was 1.8 times higher than for the reference (Fig. 8d and h). As can be seen in the corresponding SEM-micrograph (Fig. 12), a tribo-film similar to experiments with lower relative humidity was formed. However, it was only present in the edge area, while the central area of the track featured severe wear. These effects were attributed to pseudo-negative compressibility and slippage of the $Ti_3C_2T_x$–nanosheets. Similar to other hydrophilic materials such as graphite oxide [71], clay minerals [72] or layered titanite [73], the spacings of multi-layered MXene expand when quasi-hydrostatically compressed in the presence of solvents such as water due to intercalation of solvent's molecules between the weakly bonded layers [74,75]. GHIDIU et al. [76] have assigned the shear to facilitate the insertion of bilayer H_20 between the MXene-nanosheets. Thus, the separation of multi-layered $Ti_3C_2T_x$-nanosheets into disordered sheets reduced sheet–to–sheet bonding and the counter–body shifted the MXenes relatively easily from the actual

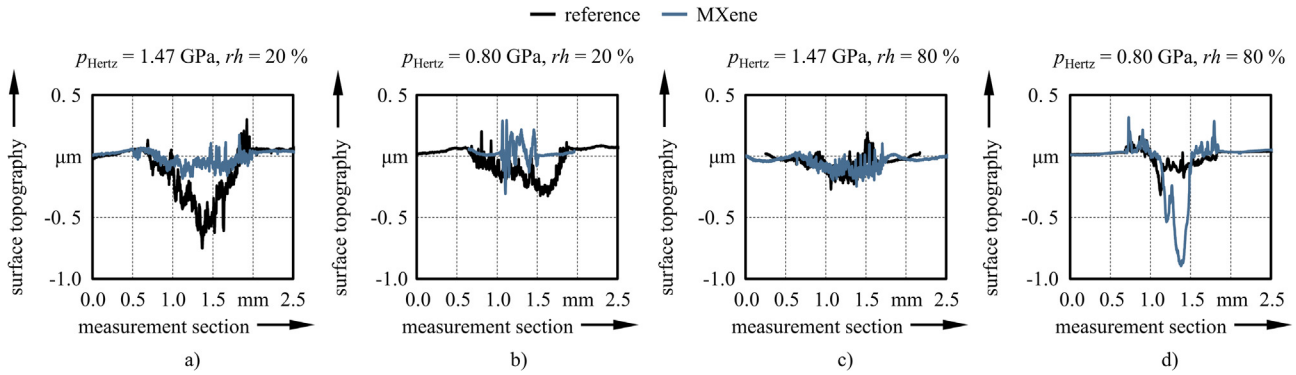

Fig. 7. Characteristic line profiles of wear tracks on the disk for reference (black) and $Ti_3C_2T_x$-coated (blue) specimens with an HERTZian pressure of p_{Hertz} = 1.47 GPa and at a relative humidity of rh = 20% (a), p_{Hertz} = 0.80 GPa and rh = 20% (b), p_{Hertz} = 1.47 GPa mm and rh = 80% (c), p_{Hertz} = 0.80 GPa and rh = 80% (d).

contact area to the inner and outer edge of the wear track. While these edge areas were still well protected by hydrated $Ti_3C_2T_x$-nanoparticles, the now exposed central area of the substrate was affected by concentrated stresses, thus leading to observed wear pattern and increased wear volume.

4. Conclusions

Accurate material characterization and tribological experiments were used to assess the friction and wear behavior of MXene–nanosheets when used as a solid lubricant dependent on the applied contact pressure and the adjusted relative humidity. In the case of a relative humidity of 20%, $Ti_3C_2T_x$-nanosheets induced a friction reduction by a factor of up to 2.3 as well as a significant reduction of substrate and counter-body volumetric wear up to a cumulated factor of 2.7. As verified by SEM and Raman spectroscopy, this was due to the in-situ formation of a tribo-film on the disks consisting of densified $Ti_3C_2T_x$-nanosheets, which was particularly pronounced for the lower initial Hertzian pressure of 0.8 GPa. Testing with higher contact pressures of 1.47 GPa led to a partial rupture of the wear-protective tribo-film, which reduced its beneficial effects, in particular, an earlier rise in friction and lower wear reduction. Moreover, no reduction in friction or wear was found for a higher relative humidity of 80%. This was attributed to the expansion of the basal spacings of the multi-layered MXenes by shear-induced slippage and intercalated H_2O-molecules.

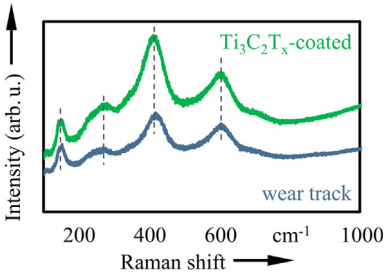

Fig. 9. Raman spectroscopy of $Ti_3C_2T_x$-coated and worn surface of the specimens with an HERTZian pressure of p_{Hertz} = 0.80 GPa and at a relative humidity of rh = 20%.

Summarizing, the obtained results strongly emphasize the

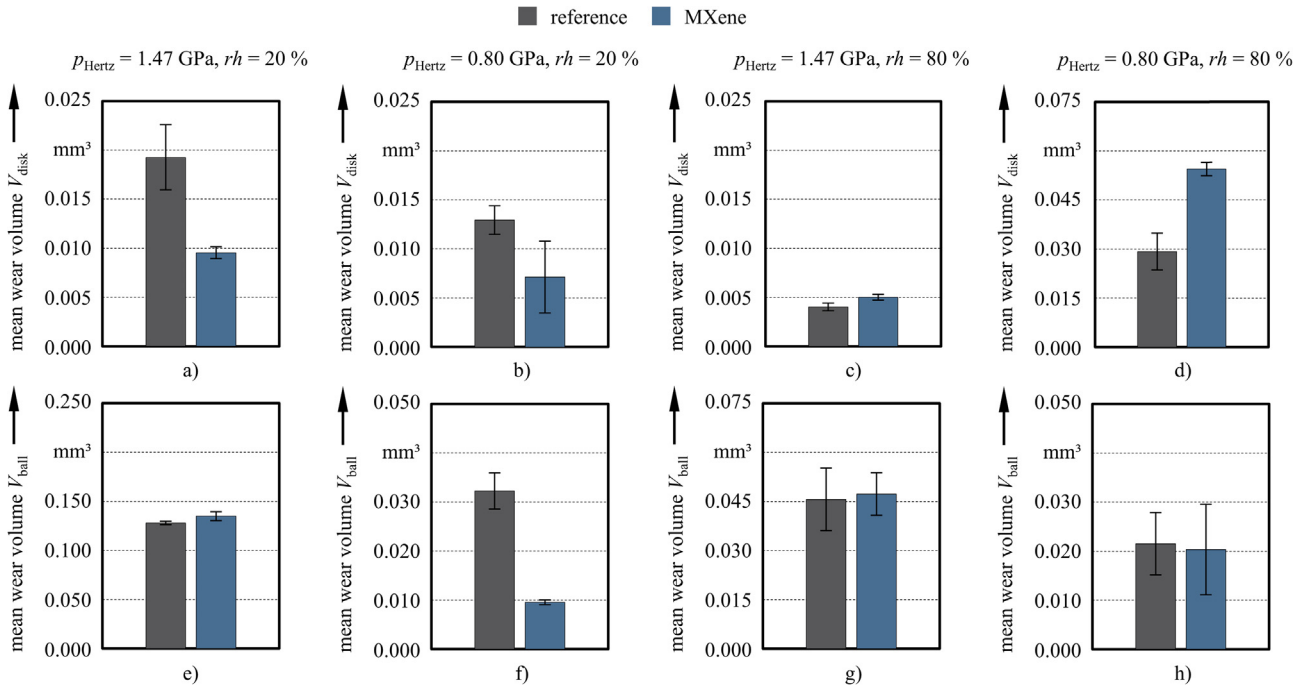

Fig. 8. Mean wear volumes (n = 3) on the disk and the balls for reference (grey) and $Ti_3C_2T_x$-coated (blue) specimens with an HERTZian pressure of p_{Hertz} = 1.47 GPa and at a relative humidity of rh = 20% (a, e), p_{Hertz} = 0.80 GPa and rh = 20% (b, f), p_{Hertz} = 1.47 GPa mm and rh = 80% (c, g), p_{Hertz} = 0.80 GPa and rh = 80% (d, h).

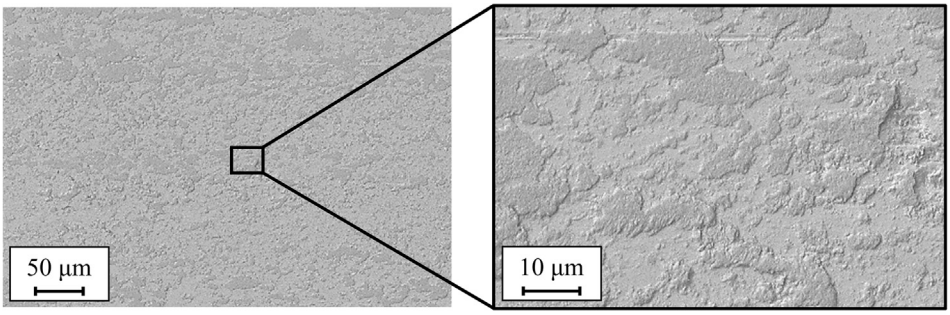

Fig. 10. SEM-micrographs of the wear track after tribological testing for a $Ti_3C_2T_x$-coated specimen with an HERTZian pressure of p_{Hertz} = 1.47 GPa and at a relative humidity of rh = 20%.

potentially outstanding wear-protective properties of $Ti_3C_2T_x$–nanosheets when used as solid lubricant in tribological systems operating under moderate contact pressures and low humidity conditions. Terminal groups and the amount of intercalated water can be considered as defining parameters to tailor the interfacial strength and thus, their friction and wear characteristics. Therefore, further research is necessary in the processing of MXene–nanosheets, thus applying them to tribological contacts. The introduction of certain ions, for instance K^+, in the MXene interlayers may inhabit this behavior by reducing H_20 mobility and maintaining sheet-to-sheet bonding [75–77].

CRediT authorship contribution statement

Max Marian: . : Conceptualization, Investigation, Writing - original draft, Visualization. **Gui Cheng Song:** Investigation, Resources. **Bo Wang:** Investigation, Resources. **Victor M. Fuenzalida:** Investigation. **Sebastian Krauss:** Investigation, Supervision. **Benoit Merle:** Investigation, Supervision. **Stephan Tremmel:** Resources, Supervision, Funding acquisition. **Sandro Wartzack:** Resources, Supervision, Funding acquisition. **Jinhong Yu:** Resources, Supervision, Funding acquisition. **Andreas Rosenkranz:** Conceptualization, Investigation, Writing - original draft, Visualization, Supervision, Funding acquisition.

Declaration of Competing Interest

The authors declare that they have no known competing financial interests or personal relationships that could have appeared to influence the work reported in this paper.

Acknowledgements

M. MARIAN, S. TREMMEL and S. WARTZACK greatly acknowledge the continious support of the technical faculty of Friedrich-Alexander-Universität (FAU) Erlangen-Nürnberg, Germany. R. ZHAO and student assistant K. FEILE from Engineering Design, FAU Erlangen-Nürnberg are kindly acknowledged for their assistance in SEM and Raman characterization, respectively. Furthermore, T. WEIKERT is thanked for the fruitful discussions. V. M. Fuenzalida greatly acknowledges the project “Núcleo Milenio Multimat”. R. ESPINOZA and N. ESCALONA from Universidad de Chile are thanked for their help in HR-TEM and TPD-MS, respectively.

Funding

This work was supported by CONICYT within the project Fondecyt 11180121 as well as the VID of the University of Chile in the framework of “U-Inicia UI013/2018".

Author contributions

M. MARIAN and A. ROSENKRANZ conceived the idea and designed the experiments. G. C. SONG, B. WANG and J. H. YU synthesized the samples, which were characterized by A. ROSENKRANZ. V. M. FUENZALIDA performed the XPS measurements. S. KRAUß and B. MERLE characterized the as-deposited coatings by FIB. The tribological experiments and data analysis were carried out by M. MARIAN and supervised by S. TREMMEL. M. MARIAN and A. ROSENKRANZ wrote the original draft of the manuscript. All authors

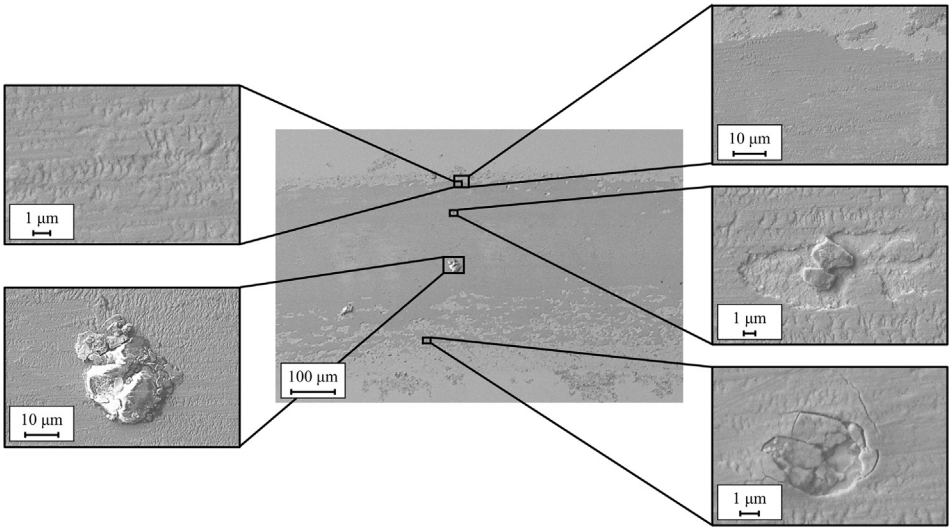

Fig. 11. SEM-micrographs of the wear track after tribological testing for a $Ti_3C_2T_x$-coated specimen with an HERTZian pressure of p_{Hertz} = 0.80 GPa and at a relative humidity of rh = 20%

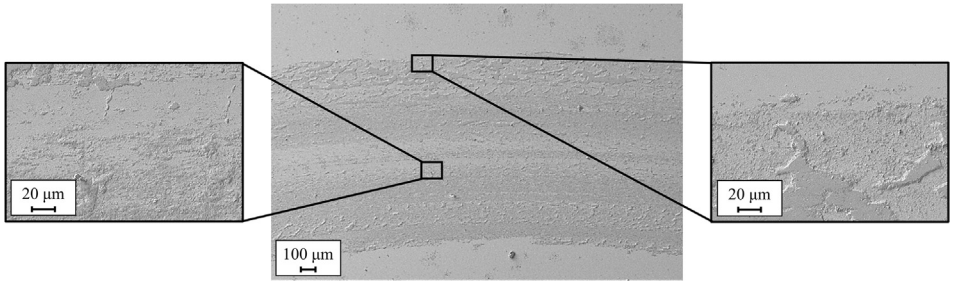

Fig. 12. SEM-micrographs of the wear track after tribological testing for a $Ti_3C_2T_x$-coated specimen with an HERTZian pressure of p_{Hertz} = 0.80 GPa and at a relative humidity of rh = 80%.

have reviewed, edited and read the manuscript as well as approved the final version.

Data availability

Upon request, the authors are pleased to provide all relevant data required to reproduce the work reported.

References

[1] K.S. Novoselov, A.K. Geim, S.V. Morozov, D. Jiang, Y. Zhang, S.V. Dubonos, I.V. Grigorieva, A.A. Firsov, Electric field effect in atomically thin carbon films, Science 306 (2004) 666–669, https://doi.org/10.1126/science.1102896.

[2] A.K. Geim, K.S. Novoselov, The rise of graphene, Nat. Mater. 6 (2007) 183–191, https://doi.org/10.1038/nmat1849.

[3] A.K. Geim, Graphene: status and prospects, Science 324 (2009) 1530–1534, https://doi.org/10.1126/science.1158877.

[4] K. Watanabe, T. Taniguchi, H. Kanda, Direct-bandgap properties and evidence for ultraviolet lasing of hexagonal boron nitride single crystal, Nat. Mater. 3 (2004) 404–409, https://doi.org/10.1038/nmat1134.

[5] C.R. Dean, A.F. Young, I. Meric, C. Lee, L. Wang, S. Sorgenfrei, K. Watanabe, T. Taniguchi, P. Kim, K.L. Shepard, J. Hone, Boron nitride substrates for high-quality graphene electronics, Nat. Nanotechnol. 5 (2010) 722–726, https://doi.org/10.1038/nnano.2010.172.

[6] J.N. Coleman, M. Lotya, A. O'Neill, S.D. Bergin, P.J. King, U. Khan, K. Young, A. Gaucher, S. De, R.J. Smith, I.V. Shvets, S.K. Arora, G. Stanton, H.-Y. Kim, K. Lee, G.T. Kim, G.S. Duesberg, T. Hallam, J.J. Boland, J.J. Wang, J.F. Donegan, J.C. Grunlan, G. Moriarty, A. Shmeliov, R.J. Nicholls, J.M. Perkins, E.M. Grieveson, K. Theuwissen, D.W. McComb, P.D. Nellist, V. Nicolosi, Two-dimensional nanosheets produced by liquid exfoliation of layered materials, Science 331 (2011) 568–571, https://doi.org/10.1126/science.1194975.

[7] Q.H. Wang, K. Kalantar-Zadeh, A. Kis, J.N. Coleman, M.S. Strano, Electronics and optoelectronics of two-dimensional transition metal dichalcogenides, Nature Nanotech 7 (11) (2012) 699–712, https://doi.org/10.1038/nnano.2012.193.

[8] M. Naguib, V.N. Mochalin, M.W. Barsoum, Y. Gogotsi, 25th anniversary article: MXenes: a new family of two-dimensional materials, Adv. Mater. Weinheim. 26 (2014) 992–1005, https://doi.org/10.1002/adma.201304138.

[9] B. Anasori, M.R. Lukatskaya, Y. Gogotsi, 2D metal carbides and nitrides (MXenes) for energy storage, Nat. Rev. Mater. 2 (2017) 16098, https://doi.org/10.1038/natrevmats.2016.98.

[10] X. Wang, S. Kajiyama, H. Iinuma, E. Hosono, S. Oro, I. Moriguchi, M. Okubo, A. Yamada, Pseudocapacitance of MXene nanosheets for high-power sodium-ion hybrid capacitors, Nat. Commun. 6 (2015) 6544, https://doi.org/10.1038/ncomms7544.

[11] F. Shahzad, M. Alhabeb, C.B. Hatter, B. Anasori, S. Man Hong, C.M. Koo, Y. Gogotsi, Electromagnetic interference shielding with 2D transition metal carbides (MXenes), Science 353 (2016) 1137–1140, https://doi.org/10.1126/science.aag2421.

[12] J. Ran, G. Gao, F.-T. Li, T.-Y. Ma, A. Du, S.-Z. Qiao, Ti3C2 MXene co-catalyst on metal sulfide photo-absorbers for enhanced visible-light photocatalytic hydrogen production, Nat. Commun. 8 (2017) 13907, https://doi.org/10.1038/ncomms13907.

[13] Z.W. Seh, K.D. Fredrickson, B. Anasori, J. Kibsgaard, A.L. Strickler, M.R. Lukatskaya, Y. Gogotsi, T.F. Jaramillo, A. Vojvodic, Two-Dimensional Molybdenum Carbide (MXene) as an Efficient Electrocatalyst for Hydrogen Evolution, ACS Energy Lett. 1 (2016) 589–594, https://doi.org/10.1021/acsenergylett.6b00247.

[14] W. Lian, Y. Mai, C. Liu, L. Zhang, S. Li, X. Jie, Two-dimensional Ti3C2 coating as an emerging protective solid-lubricant for tribology, Ceram. Int. 44 (2018) 20154–20162, https://doi.org/10.1016/j.ceramint.2018.07.309.

[15] D. Zhang, M. Ashton, A. Ostadhossein, A.C.T. van Duin, R.G. Hennig, S.B. Sinnott, Computational study of low interlayer friction in Tin + 1Cn (n = 1, 2, and 3) MXene, ACS Appl. Mater. Interfaces 9 (2017) 34467–34479, https://doi.org/10.1021/acsami.7b09895.

[16] R.M. Ronchi, J.T. Arantes, S.F. Santos, Synthesis, structure, properties and applications of MXenes: current status and perspectives, Ceram. Int. 45 (2019) 18167–18188, https://doi.org/10.1016/j.ceramint.2019.06.114.

[17] H. Zhang, L. Wang, Q. Chen, P. Li, A. Zhou, X. Cao, Q. Hu, Preparation, mechanical and anti-friction performance of MXene/polymer composites, Mater. Des. 92 (2016) 682–689, https://doi.org/10.1016/j.matdes.2015.12.084.

[18] Y.J. Mai, Y.G. Li, S.L. Li, L.Y. Zhang, C.S. Liu, X.H. Jie, Self-lubricating Ti3C2 nanosheets/copper composite coatings, J. Alloy. Compd. 770 (2019) 1–5, https://doi.org/10.1016/j.jallcom.2018.08.100.

[19] J. Yang, B. Chen, H. Song, H. Tang, C. Li, Synthesis, characterization, and tribological properties of two-dimensional Ti 3 C 2, Cryst. Res. Technol. 49 (2014) 926–932, https://doi.org/10.1002/crat.201400268.

[20] X. Zhang, M. Xue, X. Yang, Z. Wang, G. Luo, Z. Huang, X. Sui, C. Li, Preparation and tribological properties of Ti 3 C 2 (OH) 2 nanosheets as additives in base oil, RSC Adv. 5 (2015) 2762–2767, https://doi.org/10.1039/C4RA13800G.

[21] M. Xue, Z. Wang, F. Yuan, X. Zhang, W. Wei, H. Tang, C. Li, Preparation of TiO 2 /Ti 3 C 2 T x hybrid nanocomposites and their tribological properties as base oil lubricant additives, RSC Adv. 7 (2017) 4312–4319, https://doi.org/10.1039/C6RA27653A.

[22] Y. Liu, X. Zhang, S. Dong, Z. Ye, Y. Wei, Synthesis and tribological property of Ti3C2TXnanosheets, J. Mater. Sci. 52 (2017) 2200–2209, https://doi.org/10.1007/s10853-016-0509-0.

[23] A. Rosenkranz, P.G. Grützmacher, R. Espinoza, V.M. Fuenzalida, E. Blanco, N. Escalona, F.J. Gracia, R. Villarroel, L. Guo, R. Kang, F. Mücklich, S. Suarez, Z. Zhang, Multi-layer Ti3C2Tx-nanoparticles (MXenes) as solid lubricants – role of surface terminations and intercalated water, Appl. Surf. Sci. 494 (2019) 13–21, https://doi.org/10.1016/j.apsusc.2019.07.171.

[24] Y. Guo, X. Zhou, D. Wang, X. Xu, Q. Xu, Nanomechanical properties of Ti3C2 Mxene, Langmuir 35 (2019) 14481–14485, https://doi.org/10.1021/acs.langmuir.9b02619.

[25] X. Yin, J. Jin, X. Chen, A. Rosenkranz, J. Luo, Ultra-wear-resistant MXene-based composite coating via in situ formed nanostructured tribofilm, ACS Appl. Mater. Interfaces 11 (2019) 32569–32576, https://doi.org/10.1021/acsami.9b11449.

[26] M. Marian, S. Tremmel, S. Wartzack, G. Song, B. Wang, J. Yu, A. Rosenkranz, Mxene nanosheets as an emerging solid lubricant for machine elements – Towards increased energy efficiency and service life, Appl. Surf. Sci. 523 (2020) 1–8, https://doi.org/10.1016/j.apsusc.2020.146503.

[27] B.K. Yen, B.E. Schwickert, M.F. Toney, Origin of low-friction behavior in graphite investigated by surface x-ray diffraction, Appl. Phys. Lett. 84 (2004) 4702–4704, https://doi.org/10.1063/1.1760597.

[28] N. Kumar, S. Dash, A.K. Tyagi, B. Raj, Super low to high friction of turbostratic graphite under various atmospheric test conditions, Tribol. Int. 44 (2011) 1969–1978, https://doi.org/10.1016/j.triboint.2011.08.012.

[29] R.H. Savage, D.L. Schaefer, Vapor lubrication of graphite sliding contacts, J. Appl. Phys. 27 (1956) 136–138, https://doi.org/10.1063/1.1722322.

[30] R.H. Savage, Graphite lubrication, J. Appl. Phys. 19 (1948) 1–10, https://doi.org/10.1063/1.1697867.

[31] P. Egberts, Z. Ye, X.Z. Liu, Y. Dong, A. Martini, R.W. Carpick, Environmental dependence of atomic-scale friction at graphite surface steps, Phys. Rev. B 88 (2013), https://doi.org/10.1103/PhysRevB.88.035409.

[32] Z.-Y. Li, W.-J. Yang, Y.-P. Wu, S.-B. Wu, Z.-B. Cai, Role of humidity in reducing the friction of graphene layers on textured surfaces, Appl. Surf. Sci. 403 (2017) 362–370, https://doi.org/10.1016/j.apsusc.2017.01.226.

[33] S. Bhowmick, A. Banerji, A.T. Alpas, Role of humidity in reducing sliding friction of multilayered graphene, Carbon 87 (2015) 374–384, https://doi.org/10.1016/j.carbon.2015.01.053.

[34] J. Andersson, R.A. Erck, A. Erdemir, Frictional behavior of diamondlike carbon films in vacuum and under varying water vapor pressure, Surf. Coat. Technol. 163–164 (2003) 535–540, https://doi.org/10.1016/S0257-8972(02)00617-5.

[35] J. Andersson, R.A. Erck, A. Erdemir, Friction of diamond-like carbon films in different atmospheres, Wear 254 (2003) 1070–1075, https://doi.org/10.1016/S0043-1648(03)00336-3.

[36] A. Erdemir, The role of hydrogen in tribological properties of diamond-like carbon films, Surf. Coat. Technol. 146–147 (2001) 292–297, https://doi.org/10.1016/S0257-8972(01)01417-7.

[37] H.I. Kim, J.R. Lince, O.L. Eryilmaz, A. Erdemir, Environmental effects on the friction of hydrogenated DLC films, Tribol. Lett. 21 (2006) 51–56, https://doi.org/10.1007/s11249-005-9008-1.

[38] B. Vierneusel, T. Schneider, S. Tremmel, S. Wartzack, T. Gradt, Humidity resistant MoS2 coatings deposited by unbalanced magnetron sputtering, Surf. Coat. Technol.

235 (2013) 97–107, https://doi.org/10.1016/j.surfcoat.2013.07.019.
[39] H.S. Khare, D.L. Burris, The effects of environmental water and oxygen on the temperature-dependent friction of sputtered molybdenum disulfide, Tribol Lett 52 (2013) 485–493, https://doi.org/10.1007/s11249-013-0233-8.
[40] M. Uemura, K. Saito, K. Nakao, A mechanism of vapor effect on friction coefficient of molybdenum disulfide, Tribol. Trans. 33 (1990) 551–556, https://doi.org/10.1080/10402009008981988.
[41] R.P. Pardee, The effect of humidity on low-load frictional properties of a bonded solid film lubricant, A S L E Transactions 15 (1972) 130–142, https://doi.org/10.1080/05698197208981409.
[42] A.J. Barthel, J. Luo, S.H. Kim, Origin of ultra-low friction of boric acid: role of vapor adsorption, Tribol Lett 58 (2015) 197, https://doi.org/10.1007/s11249-015-0512-7.
[43] H. Li, X.C. Zeng, Wetting and interfacial properties of water nanodroplets in contact with graphene and monolayer boron-nitride sheets, ACS Nano 6 (2012) 2401–2409, https://doi.org/10.1021/nn204661d.
[44] J.M. Martin, T. Le Mogne, C. Chassagnette, M.N. Gardos, Friction of hexagonal boron nitride in various environments, Tribol. Trans. 35 (1992) 462–472, https://doi.org/10.1080/10402009208982144.
[45] C.J. Reeves, P.L. Menezes, M.R. Lovell, T.-C. Jen, Tribology of Solid Lubricants, in: P.L. Menezes, M. Nosonovsky, S.P. Ingole, S.V. Kailas, M.R. Lovell (Eds.), Tribology for Scientists and Engineers, Springer New York, New York, NY, 2013, pp. 447–494.
[46] J.K. Lancaster, A review of the influence of environmental humidity and water on friction, lubrication and wear, Tribol. Int. 23 (1990) 371–389, https://doi.org/10.1016/0301-679X(90)90053-R.
[47] Z. Chen, X. He, C. Xiao, S. Kim, Effect of humidity on friction and wear—a critical review, Lubricants 6 (2018) 74, https://doi.org/10.3390/lubricants6030074.
[48] ISO, 683-17:1999(E) Heat-treated steels, alloy steels and free-cutting steels – Part 17: Ball and roller bearing steel.
[49] DIN EN ISO, 4288:1998-04 Geometrical Product Specifications (GPS) – Surface texture: Profile method - Rules and procedures for the assessment of surface texture.
[50] ISO, 3290-1:2014-09 Rolling bearings - Balls - Part 1: Steel balls.
[51] DIN EN, 1071-13:2010-07 Advanced technical ceramics – Methods of test for ceramic coatings – Part 13: Determination of wear rate by the pin-on-disk method.
[52] M. Hu, T. Hu, Z. Li, Y. Yang, R. Cheng, J. Yang, C. Cui, X. Wang, Surface functional groups and interlayer water determine the electrochemical capacitance of Ti3C2 T x MXene, ACS Nano 12 (2018) 3578–3586, https://doi.org/10.1021/acsnano.8b00676.
[53] M.V. Kuznetsov, S.V. Borisov, O.P. Shepatkovskii, Y.G. Veksler, V.L. Kozhevnikov, Investigation of TiC-C coatings by X-ray photoelectron spectroscopy, J. Synch. Investig. 3 (2009) 331–337, https://doi.org/10.1134/S102745100903001X.
[54] A.A. Galuska, J.C. Uht, N. Marquez, Reactive and nonreactive ion mixing of Ti films on carbon substrates, J. Vacuum Sci. Technol. A: Vacuum, Surfaces, and Films 6 (1988) 110–122, https://doi.org/10.1116/1.574992.
[55] J. Halim, K.M. Cook, M. Naguib, P. Eklund, Y. Gogotsi, J. Rosen, M.W. Barsoum, X-ray photoelectron spectroscopy of select multi-layered transition metal carbides (MXenes), Appl. Surf. Sci. 362 (2016) 406–417, https://doi.org/10.1016/j.apsusc.2015.11.089.
[56] T. Hu, J. Wang, H. Zhang, Z. Li, M. Hu, X. Wang, Vibrational properties of Ti3C2 and Ti3C2T2 (T = O, F, OH) monosheets by first-principles calculations: a comparative study, Phys. Chem. Chem. Phys. 17 (2015) 9997–10003, https://doi.org/10.1039/C4CP05666C.
[57] J.F. Moulder, W.F. Stickle, P.E. Sobol, K.D. Bomben, Handbook of X-ray photoelectron spectroscopy: A reference book of standard spectra for identification of XPS data, Perkin-Elmer, Minsesota, op. 1992.
[58] T. Tanuma, H. Okamoto, K. Ohnishi, S. Morikawa, T. Suzuki, Partially fluorinated metal oxide catalysts for a Friedel–Crafts-type reaction of dichlorofluoromethane with tetrafluoroethylene, Catal Lett 136 (2010) 77–82, https://doi.org/10.1007/s10562-009-0197-3.
[59] M.C. Biesinger, L.W.M. Lau, A.R. Gerson, R.S.C. Smart, Resolving surface chemical states in XPS analysis of first row transition metals, oxides and hydroxides: Sc, Ti, V, Cu and Zn, Appl. Surf. Sci. 257 (2010) 887–898, https://doi.org/10.1016/j.apsusc.2010.07.086.
[60] X. Zhang, Y. Liu, S. Dong, Z. Ye, Y. Guo, One-step hydrothermal synthesis of a TiO2-Ti3C2Tx nanocomposite with small sized TiO2 nanoparticles, Ceram. Int. 43 (2017) 11065–11070, https://doi.org/10.1016/j.ceramint.2017.05.151.
[61] M.A. Hope, A.C. Forse, K.J. Griffith, M.R. Lukatskaya, M. Ghidiu, Y. Gogotsi, C.P. Grey, NMR reveals the surface functionalisation of Ti3C2 MXene, Phys. Chem. Chem. Phys. 18 (2016) 5099–5102, https://doi.org/10.1039/C6CP00330C.
[62] V. Rives, Characterisation of layered double hydroxides and their decomposition products, Mater. Chem. Phys. 75 (2002) 19–25, https://doi.org/10.1016/S0254-0584(02)00024-X.
[63] D. Klaffke, On the repeatability of friction and wear results and on the influence of humidity in oscillating sliding tests of steel-steel pairings, Wear 189 (1995) 117–121, https://doi.org/10.1016/0043-1648(95)06672-1.
[64] M. Woydt, H. Mohrbacher, Niobium Carbide (NbC) As Wear Resistant Hardmetal In Opened And Closed Tribosystems, in: ABM Proceedings, Foz do Iguaçu - Brasil, Editora Blucher, São Paulo, 03.11.2014 - 05.11.2014, pp. 3842–3851.
[65] G. Bregliozzi, A. Di Schino, J.M. Kenny, H. Haefke, Influence of atmospheric humidity and grain size on the friction and wear of high nitrogen austenitic stainless steel, J. Mater. Sci. 39 (2004) 1481–1484, https://doi.org/10.1023/B:JMSC.0000013923.41628.69.
[66] P. de Baets, G. Kalacska, K. Strijckmans, F. van de Velde, A.P. van Peteghem, Experimental study by means of thin layer activation of the humidity influence on the fretting wear of steel surfaces, Wear 216 (1998) 131–137, https://doi.org/10.1016/S0043-1648(97)00189-0.
[67] H. Goto, D.H. Buckley, The influence of water vapour in air on the friction behaviour of pure metals during fretting, Tribol. Int. 18 (1985) 237–245, https://doi.org/10.1016/0301-679X(85)90069-6.
[68] Y. Wang, T. Lei, J. Liu, Tribo-metallographic behavior of high carbon steels in dry sliding, Wear 231 (1999) 1–11, https://doi.org/10.1016/S0043-1648(99)00115-5.
[69] Y. Wang, T. Lei, Wear behavior of steel 1080 with different microstructures during dry sliding, Wear 194 (1996) 44–53, https://doi.org/10.1016/0043-1648(95)06705-1.
[70] H.-K. Oh, K.-H. Yeon, H. Yun Kim, The influence of atmospheric humidity on the friction and wear of carbon steels, J. Mater. Process. Technol. 95 (1999) 10–16, https://doi.org/10.1016/S0924-0136(99)00259-9.
[71] A.V. Talyzin, V.L. Solozhenko, O.O. Kurakevych, T. Szabó, I. Dékány, A. Kurnosov, V. Dmitriev, Colossal pressure-induced lattice expansion of graphite oxide in the presence of water, Angew. Chem. Int. Ed Engl. 47 (2008) 8268–8271, https://doi.org/10.1002/anie.200802860.
[72] S. You, D. Kunz, M. Stöter, H. Kalo, B. Putz, J. Breu, A.V. Talyzin, Pressure-induced water insertion in synthetic clays, Angew. Chem. Int. Ed Engl. 52 (2013) 3891–3895, https://doi.org/10.1002/anie.201210060.
[73] S. Nakano, T. Sasaki, K. Takemura, M. Watanabe, Pressure-Induced Intercalation of Alcohol Molecules into a Layered Titanate, Chem. Mater. 10 (1998) 2044–2046, https://doi.org/10.1021/cm980273h.
[74] M. Ghidiu, M.R. Lukatskaya, M.-Q. Zhao, Y. Gogotsi, M.W. Barsoum, Conductive two-dimensional titanium carbide 'clay' with high volumetric capacitance, Nature 516 (2014) 78–81, https://doi.org/10.1038/nature13970.
[75] M. Ghidiu, J. Halim, S. Kota, D. Bish, Y. Gogotsi, M.W. Barsoum, Ion-exchange and cation solvation reactions in Ti 3 C 2 MXene, Chem. Mater. 28 (2016) 3507–3514, https://doi.org/10.1021/acs.chemmater.6b01275.
[76] M. Ghidiu, S. Kota, V. Drozd, M.W. Barsoum, Pressure-induced shear and interlayer expansion in Ti3C2 MXene in the presence of water, Sci. Adv. 4 (2018) eaao6850, https://doi.org/10.1126/sciadv.aao6850.
[77] N.C. Osti, M. Naguib, A. Ostadhossein, Y. Xie, P.R.C. Kent, B. Dyatkin, G. Rother, W.T. Heller, A.C.T. van Duin, Y. Gogotsi, E. Mamontov, Effect of metal ion intercalation on the structure of MXene and water dynamics on its internal surfaces, ACS Appl. Mater. Interfaces 8 (2016) 8859–8863, https://doi.org/10.1021/acsami.6b01490.